ISSN 1027-5495. Functional Materials, 25, No.4 (2018), p. 658-664.
doi:https://doi.org/10.15407/fm25.04.658

Mixed ZnS_xSe_{1-x} crystals for digital radiography detectors

***O.G.Trubaieva*[1], *M.A.Chaika*[2], *W.Paszkowicz*[3]**

[1]Institute for Scintillation Materials, STC "Institute for Single Crystals", National Academy of Sciences of Ukraine, 60 Nauky Ave., 61072 Kharkiv, Ukraine
[2]Institute of Low Temperature and Structure Research, Polish Academy of Sciences, Okolna 2, 50422 Wroclaw, Poland
[3]Institute of Physics, Polish Academy of Sciences, 32/46 Lotnikow al., 02-668 Warsaw, Poland

Received November 1, 2018

A possibility to use ZnS_xSe_{1-x} as a material for detection of X-ray and alpha particles has been studied. The influence of the sulphur content on the properties of ZnS_xSe_{1-x} crystals is analyzed. The bulk ZnS_xSe_{1-x} crystals were obtained by Bridgman-Stockbarger method. Six different plates cut off from the crystals with x from 0.07 to 0.39 were studied. It is found that intensity of X-ray luminescence spectra of ZnS_xSe_{1-x} plates increases with increasing sulfur content, reaching the maximum value for $ZnS_{0.22}Se_{0.78}$ composition. The scintillation light output of ZnS_xSe_{1-x} plates is shown to be higher than for commercial ZnSe(Te) and ZnSe(Al) crystals.

Keywords: ZnS_xSe_{1-x} bulk crystals, radiation detectors, alpha detector, scintillators, X-ray luminescence.

Смешанные кристаллы ZnS_xSe_{1-x} являются перспективными материалами для рентгеновских и альфа детекторов. В работе исследуется и обсуждается влияние содержания серы на сцинтилляционные свойства кристаллов ZnS_xSe_{1-x}. Объемные кристаллы ZnS_xSe_{1-x} получены методом Бриджмена-Стокбаргера. Изучено шесть различных пластинок, отрезанных от кристаллов (x от 0,07 до 0,39). Обнаружено, что интенсивность спектров рентгенолюминесценции пластин ZnS_xSe_{1-x} возрастает с увеличением содержания серы, достигая максимального значения для состава $ZnS_{0,22}Se_{0,78}$. Показано, что световыход пластин ZnS_xSe_{1-x} выше, чем для коммерческих кристаллов ZnSe(Te) и ZnSe(Al).

Змішані кристали $ZnS_{1-x}Se_x$ для детекторів цифрової радіографії. *О.Г.Трубаєва, М.А.Чайка, W.Paszkowicz.*

Змішані кристали ZnS_xSe_{1-x} є перспективними матеріалами для рентгенівських і альфа детекторів. У роботі досліджується і обговорюється вплив вмісту сірки на сцинтиляційні властивості кристалів ZnS_xSe_{1-x}. Об'ємні кристали ZnS_xSe_{1-x} отримано методом Бріджмена-Стокбаргера. Вивчено шість різних пластинок, відрізаних від кристалів (x від 0,07 до 0,39). Виявлено, що інтенсивність спектрів рентгенолюмінесценції пластин ZnS_xSe_{1-x} зростає зі збільшенням вмісту сірки, досягаючи максимального значення для складу $ZnS_{0,22}Se_{0,78}$. Показано, що світловихід пластин ZnS_xSe_{1-x} вище, ніж для комерційних кристалів ZnSe(Te) і ZnSe(Al).

1. Introduction

ZnSe, ZnSe(Al), ZnSe(Te), CsI(Tl), NaI(Tl), and ZnS(Ag) are widely used for development of optoelectronic, light emitting and light detecting devices, gamma cameras, solar cells and scintillators for X-ray, γ-ray and alpha particles detection [1–5]. However, all those crystals have a number of shortcomings. In particular, ZnSe crystals have a low light output, and ZnSe(Al) ones a high thermal quenching factor [6]. The luminescence kinetics in ZnSe(Te) crystals is "slow": up to a hundred microseconds. Scintillators based on CsI(Tl) and NaI(Tl) are hygroscopic and require the additional moisture protection [7]. The shortcoming of ZnS(Ag)-based crystals consists in that they badly transmit photons of visible light and can only be used as thin layers [8].

Mixed ZnS_xSe_{1-x} scintillators could reduce of these disadvantages [9–12]. The main advantage of ZnS_xSe_{1-x} crystals is a presence of continuous series of solid solutions over an entire composition range [13, 14]. So, both optical and scintillation characteristics of ZnS_xSe_{1-x} crystals can be tuned by proper selected of x value.

Variation of ZnS_xSe_{1-x} composition allows optimizing the luminescence spectrum for better match with conventional image sensors, as well as improving thermal stability of the output parameters in ZnS_xSe_{1-x} crystals. Moreover, ZnS_xSe_{1-x} scintillation materials have better transparency to their own radiation. Also, position of the energy levels of radiative recombination centres in the bandgap of ZnS_xSe_{1-x} crystals can be easily tuned [15–17].

Multiple studies were dedicated to obtaining ZnS_xSe_{1-x} mixed crystals (for examples [9–14, 18–21]), most of them using vapour phase growth methods, and only a few teams have obtained ZnS_xSe_{1-x} crystals by the directional solidification [18–20]. The directional solidification techniques allow obtaining large ZnS_xSe_{1-x} mixed crystals for detectors of high-energy particles. However, for practical use the knowledge about structure and optical properties of ZnS_xSe_{1-x} bulk crystals is required. Moreover, the advantages of ZnS_xSe_{1-x} scintillators over their analogues (ZnSe(Al) and ZnSe(Te)) needs additional experimental evidences.

In this paper we studied the scintillation and optical properties of bulk ZnS_xSe_{1-x} crystals taking their possible application as X-ray and alpha-particle detectors into account. A special attention was paid to the comparison of the properties of ZnS_xSe_{1-x} and commercial ZnSe, ZnSe(Al), ZnSe(Te) scintillators.

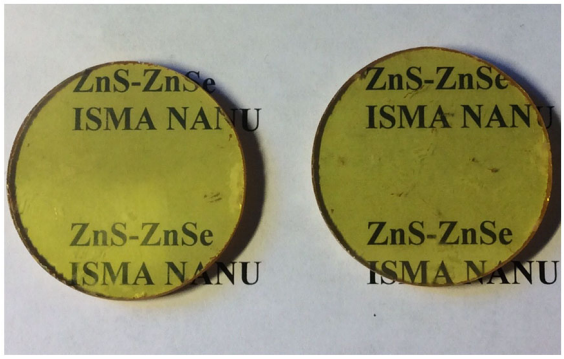

Fig. 1. Photograph of the mirror-polished ZnS_xSe_{1-x} plates.

Table 1. Nominal and measurement compositions of ZnS_xSe_{1-x} crystals and plates from these crystals

Crystal name	plates	
	nominal compositions	measurement compositions
C1	$ZnS_{0.05}Se_{0.95}$	$ZnS_{0.07}Se_{0.93}$
C2	$ZnS_{0.1}Se_{0.9}$	$ZnS_{0.15}Se_{0.85}$
C3	$ZnS_{0.15}Se_{0.85}$	$ZnS_{0.22}Se_{0.78}$
C4	$ZnS_{0.2}Se_{0.8}$	$ZnS_{0.28}Se_{0.72}$
C5	$ZnS_{0.25}Se_{0.75}$	$ZnS_{0.32}Se_{0.68}$
C6	$ZnS_{0.3}Se_{0.7}$	$ZnS_{0.39}Se_{0.61}$

2. Experimental

The current investigations involved six ZnS_xSe_{1-x} crystals of various S/Se ratios, grown by Bridgman-Stockbarger method. The Bridgman-Stockbarger method allows for obtaining large ZnS_xSe_{1-x} crystals with relatively high growing speed as compared to other directional solidifications techniques. ZnS_xSe_{1-x} bulk crystals were grown from pre-sintered charge of nominal x = 0.05; 0.1; 0.15; 0.2; 0.25 and 0.3.

Before the growth, the raw materials were annealed in a quartz crucible at 1170 K during 5 h in hydrogen atmosphere for removing oxygen impurites. The crystal growth was carried out in graphite crucibles with the diameter of 25 mm under Ar pressure $P_{Ar} = 2 \cdot 10^6$ Pa, the crystallization rate was equal to 7 mm/h, the heater temperature was in the range from 1870 to 2000 K depending on the composition of the initial raw materials.

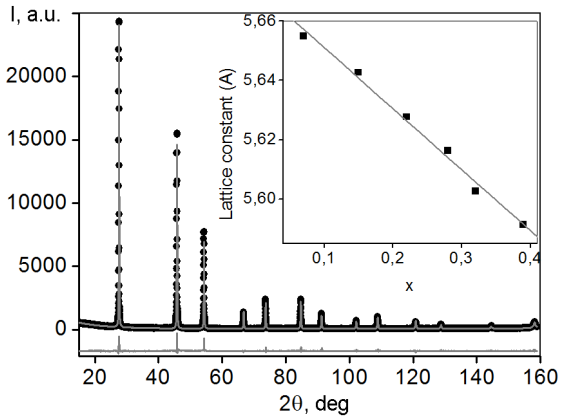

Fig. 2. Result of Rietveld refinement for a powder diffraction pattern of $ZnS_{0.32}Se_{0.68}$ (C5) plate. Crosses denote experimental points, and the solid line is the calculated pattern. The difference pattern is shown in the lower part of the figure. The inset illustrates the dependence of lattice constant of ZnS_xSe_{1-x} plates from compositions.

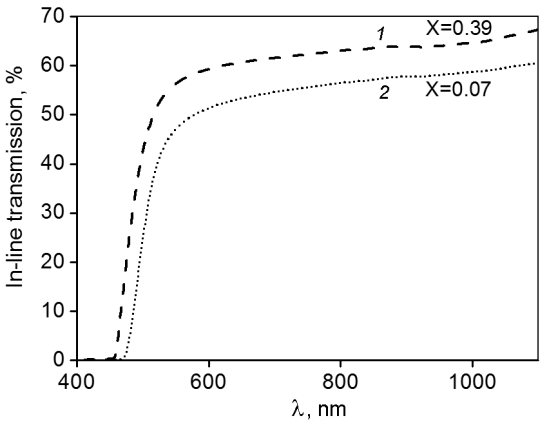

Fig. 3. Optical in-line transmission spectra for a) $ZnS_{0.39}Se_{0.61}$ (C6), b) $ZnS_{0.07}Se_{0.93}$ (C1) crystals.

The mixed crystals with nominal compositions x listed in the Table 1 were cut perpendicular to the growth direction to prepare plates with diameter of 25 mm and thickness of 4 mm (see Fig. 1). Properties of ZnS_xSe_{1-x} crystals were compared with properties of ZnSe, ZnSe(Al), ZnSe(Te) crystals grown in the similar conditions (for more details see [1, 2]). Most investigations were provided on the one plate selected from each of ZnSe, ZnSe(Al), ZnSe(Te) and six ZnS_xSe_{1-x} crystals. After the growth, the chemical analysis of ZnS_xSe_{1-x} plates was carried out in order to determine the content of the cationic impurities, as well as the actual composition of the crystals. As a result, six different plates were studied with the following compositions: $ZnS_{0.07}Se_{0.93}$, $ZnS_{0.15}Se_{0.85}$, $ZnS_{0.22}Se_{0.78}$, $ZnS_{0.28}Se_{0.72}$, $ZnS_{0.32}Se_{0.68}$, $ZnS_{0.39}Se_{0.61}$. It should be noted, that segregation coefficient was measurement by investigations of whole plates for each crystals.

The plates were annealed in zinc vapour (T = 1223 K, $P_{Zn} = 5 \cdot 10^7$ Pa, t = 48 h); annealing was used to provide the final formation of luminescent centres, as well as for suppression of nonradiative relaxation channels [1, 2]. To carry out the study of the luminescent properties the surfaces of the plates were polished by diamond powder. In the Fig. 1 the photograph of the mirror-polished ZnS_xSe_{1-x} plates is shown.

X-ray luminescence of the plates was excited by REIS-I X-ray source (Cu, U = 10–45 kV). The emission spectra were analyzed using KSVU-23 spectrophotometer. For the measurements of the relative light output and afterglow level η (%) X-ray tube with tungsten anode and silicon photodiode (PD-24 Smiths Heimann AMS-1) was used with subsequent automatic mathematical processing of the data.

The transmission spectra were measured using single-beam spectrophotometer Shimadzu UVmini-1240. X-ray diffraction measurements were done with $CuK_{\alpha 1}$ radiation using a Bragg-Brentano powder diffractometer (X'Pert Pro Alpha1MPD from Philips/PANalytical) equipped by an incident beam Ge(111) Johansson monochromator and a strip detector. Data processing was carried out using a FullProf 3.0 program.

Measurements of the technical light output was carried out at excitation of the plates by γ-ray sources of alpha particles ^{239}Pu (E_α = 5156 keV) at the working temperature of 294 K. As a photodetector, R1307 photomultiplier tube was used. The GOST 17038.2-79 was used as standard [22].

3. Results and discussion

3.1 X-ray diffraction

According to X-ray diffraction (XRD) results, all ZnS_xSe_{1-x} plates possess the structure of pure ZnSe without any additional peaks (Fig. 2). The experimental lattice constants of $ZnS_{0.07}Se_{0.93}$ (C1), $ZnS_{0.15}Se_{0.85}$ (C2), $ZnS_{0.22}Se_{0.78}$ (C3), $ZnS_{0.28}Se_{0.72}$ (C4), $ZnS_{0.32}Se_{0.68}$ (C5), and $ZnS_{0.39}Se_{0.61}$ (C6) plates were 5.6550, 5.6427, 5.6277, 5.6164, 5.6026 and 5.5913 Å, respectively with standard deviations ±+0.0001 Å. The lattice constant of the ZnS_xSe_{1-x} plates was de-

creased with increasing of the sulfur content. In this case, the reflections of X-ray diffraction patterns shift systematically to larger angles (see Inset in Fig. 2).

The lattice constants of ZnS_xSe_{1-x} plates were fitted by means of Vegard's rule:

$$a(ZnS_xSe_{1-x}) = \\ = x \cdot a(ZnS) + (1 - x) \cdot a(ZnSe), \quad (1)$$

where x is the concentration of sulfur, a(ZnS) and a(ZnSe) is the lattice constants off pure ZnS, and ZnSe, respectively, b is the bowing parameter of the deviation of the lattice constant of ZnS_xSe_{1-x} plates from a linear variation versus composition [23]. Our experimental data of lattice parameter is well fitted by the Eq. 1, the difference between experimental and theoretical calculations was not larger than 0.001 Å. The lattice constants of pure ZnS (5.465 Å) and ZnSe (5.660 Å) compounds were calculated by used Vegard's rule. The calculated values of the lattice constant for ZnS and ZnSe is close to the values reported for these crystals (5.372 Å and 5.670 Å, respectively) [24].

3.2 Transmission and optical bandgap

Optical investigations were carried out at room temperature for ZnS_xSe_{1-x} plates with different compositions. The transmission spectra of ZnS_xSe_{1-x} plates are shown in Fig. 3. For ZnS_xSe_{1-x} plates the transmittance at $\lambda = 600$ nm was in the range from 60 % (for $ZnS_{0.39}Se_{0.61}$ (C6)) to 51 % (for $ZnS_{0.07}Se_{0.93}$ (C1)), the thickness of the plates were 4 mm.

Incorporations of sulphur into ZnSe can lead to appearance of defects of different types or change the type of chemical bonds which, in turn, have an influence on the width of the optical bandgap in ZnS_xSe_{1-x} bulk crystals [25, 26]. The values of optical bandgaps of ZnS_xSe_{1-x} plates were determined by optical spectroscopy methods (for the method see [27]).

Values of the optical bandgaps for a) $ZnS_{0.07}Se_{0.93}$ (C1), b) $ZnS_{0.15}Se_{0.85}$ (C2), c) $ZnS_{0.22}Se_{0.78}$ (C3), d) $ZnS_{0.28}Se_{0.72}$ (C4), e) $ZnS_{0.32}Se_{0.68}$ (C5), f) $ZnS_{0.39}Se_{0.61}$ (C6) plates were 2.59, 2.63, 2.68, 2.70, 2.73 and 2.78 eV, respectively. The transmission spectra of ZnS_xSe_{1-x} plates were measured five times in different parts of the plates, the standard deviation was estimated as 0.01 eV. Dependence of the bandgap on the concentration of sulfur was fitted according to Eq. (2):

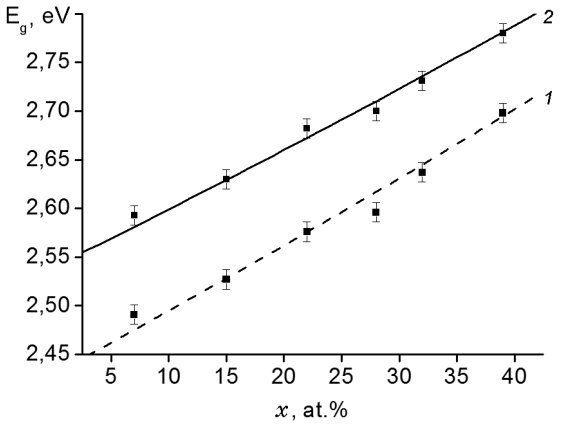

Fig. 4. The dependences of the energy of the band gap (eV) on the concentration of sulfur in (*1*) indirect and (*2*) direct transitions for bulk ZnS_xSe_{1-x} crystals, where $x = 0.07$–0.39. The points indicate the experimental results; the solid and dashed straight lines represent the dependences calculated in accordance with equation (2).

$$E_g(x) \approx \\ \approx x \cdot E_A + (1 - x) \cdot E_B - b \cdot x \cdot (1 - x), \quad (2)$$

where x is the concentration of sulfur, E_A is the bandgap of pure ZnS, E_B is the bandgap of pure ZnSe, b is the bowing coefficient. The optical bowing parameter b for ZnS_xSe_{1-x} plates is 0.1 falling into the range of previously reported optical bowing parameters (0–0.63) [24].

The energies of the bandgaps for pure ZnS, ZnSe and $ZnS_{0.4}Se_{0.6}$ compounds were calculated by means of Eq. (2), and are 3.22 eV, 2.54 and 2.8 eV, respectively. The estimated value of the bandgap energy was lower than common reported in literature, for example the bandgap of pure ZnS — 3.0 [24] and 2.65 eV [14], ZnSe — 3.65 [24] and 3.6 [14], $ZnS_{0.4}Se_{0.6}$ — 2.9 [24] and 3.2 eV [14]. These differences could be caused by using of various methods — vapour phase growth methods [24] solid state reactions [14] and grow from melt (Fig. 4). The calculated values of the optical bandgaps for ZnS and ZnSe in our case is close to the values reported for the bulk crystals (3.54 and 2.58 eV, respectively) [28, 29] which indicate high quality of these crystals. The estimated too small value of energy gap of ZnS is probably caused by not correctly estimated of bowing parameter due to lack of experimental data for large S

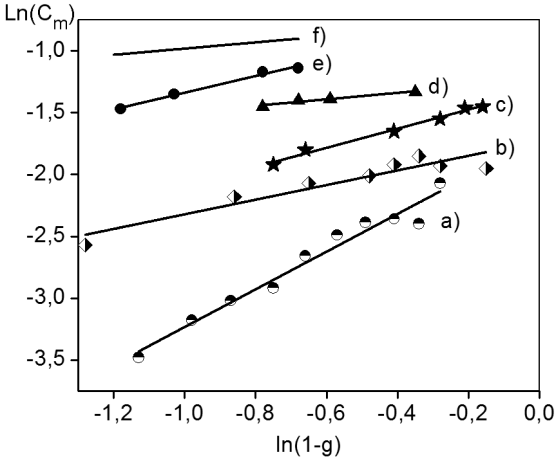

Fig. 5. The longitudinal distribution of sulfur in ZnS_xSe_{1-x} crystals as a function of solidified fraction for: a) C1, b) C2, c) C3, d) C4, e) C5, f) C6 nominal compositions.

content in the crystal. An increase of the sulfur content in ZnS_xSe_{1-x} bulk crystal leads to increase of the bandgap. Continuous change of the bandgap of ZnS_xSe_{1-x} crystals with their composition indicates absence of any new (defect) levels in the bandgap. Wider bandgap and higher atomic mass ratio for ZnS_xSe_{1-x} as compared to ZnSe(Te) or/and ZnSe(Al) crystals extend application areas of such semiconductor.

3.3 Segregation coefficient

Longitudinal distribution of impurities is one of the features of mixed crystals grown by directional solidification. The effective segregation coefficients of sulfur in ZnS_xSe_{1-x} bulk crystals are necessary for designing the melt composition.

According to the model of Burton, Prim and Slichter, the effective segregation coefficient can be calculated by:

$$\ln(C_m) = (K_{eff} - 1)\ln(1 - g) + \ln(K_{eff} \cot C_0), \quad (3)$$

where C_m, C_0 are the sulfur concentrations in the mixed crystal and the initial melt, respectively, g is the solidification fraction of melts, and K_{eff} — the segregation coefficient. Concentration of sulfur in each ZnS_xSe_{1-x} plate was determined by means of optical spectroscopy using Eq. 3. Dependence of $\ln(C_m)$ on $\ln(1-g)$ is shown in the Fig. 5, K_{eff} was obtained from the slope of the straight line [30].

Segregation coefficient determines the behaviour of impurities during crystallization and their distribution within the

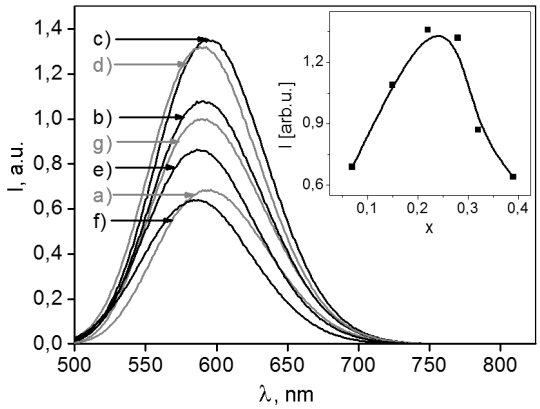

Fig. 6. Normalized X-ray luminescence spectra of ZnS_xSe_{1-x} plates after annealing in Zn vapour: a) $ZnS_{0.07}Se_{0.93}$ (C1), b) $ZnS_{0.15}Se_{0.85}$ (C2), c) $ZnS_{0.22}Se_{0.78}$ (C3), d) $ZnS_{0.28}Se_{0.72}$ (C4), e) $ZnS_{0.32}Se_{0.68}$ (C5), f) $ZnS_{0.39}Se_{0.61}$ (C6), and g) ZnSe(Al). Inset show dependence of intensity luminescence band on the composition of ZnS_xSe_{1-x} plates.

crystal. This coefficient depends on a number of factors: nature of impurities and host materials, crystallization conditions (speed and intensity of mixing), but, first of all, on the type of phase diagram. The segregation coefficients of sulfur in crystals C1, C2, C3, C4, C5 and C6 were 2.5, 1.5, 1.8, 1.3, 1.7, 1.2, respectively. For all the crystals, the segregation coefficient is more than one indicating good solubility of sulfur in the solid phase and increase of the melting point of ZnS_xSe_{1-x} bulk crystals with increasing sulfur content.

3.4 X-ray luminescence and light output

Light generation in ZnS_xSe_{1-x} plates during relaxation of the energy of initial X-ray or γ-ray quanta occurs through energy levels of crystal defects. These defects can be identified by X-ray luminescence spectroscopy. The normalized X-ray luminescence spectra of ZnS_xSe_{1-x} plates are shown in Fig. 6. It was shown that the spectra of ZnS_xSe_{1-x} mixed plates consist of a single luminescence band with maximum in the range from 591 to 584 nm. The normalized intensity of X-ray luminescence increases with the sulfur content and reaches a maximum for the composition $ZnS_{0.22}Se_{0.78}$. This occurs owing to the formation of an optimal number of ternary complexes $V_{Zn}Zn_iO_{Se}$ in those crystals (see the inset in Fig. 6). Increase of sulfur concentration leads to the shift of the luminescence band maximum to the short-wavelength region. This shift is determined by displacement of the fundamental

Table 2. Light output of of ZnS_xSe_{1-x} plates at X-ray excitation

Plates	Relative light output, %	Afterglow, %		
		5 ms	15 ms	25 ms
$ZnS_{0.07}Se_{0.93}$ (C1)	98	0.24	<0.02	<0.02
$ZnS_{0.15}Se_{0.85}$ (C2)	84	0.15	<0.02	<0.02
$ZnS_{0.22}Se_{0.78}$ (C3)	159	0.40	<0.02	<0.02
$ZnS_{0.28}Se_{0.72}$ (C4)	122	0.54	<0.02	<0.02
$ZnS_{0.32}Se_{0.68}$ (C5)	103	0.37	<0.02	<0.02
$ZnS_{0.39}Se_{0.61}$ (C6)	136	0.46	0.07	<0.02
ZnSe(Te)	100	0.30	0.17	<0.02
ZnSe(Al)	95	0.40	<0.02	<0.02
ZnS	75	58.04	39.74	31.77

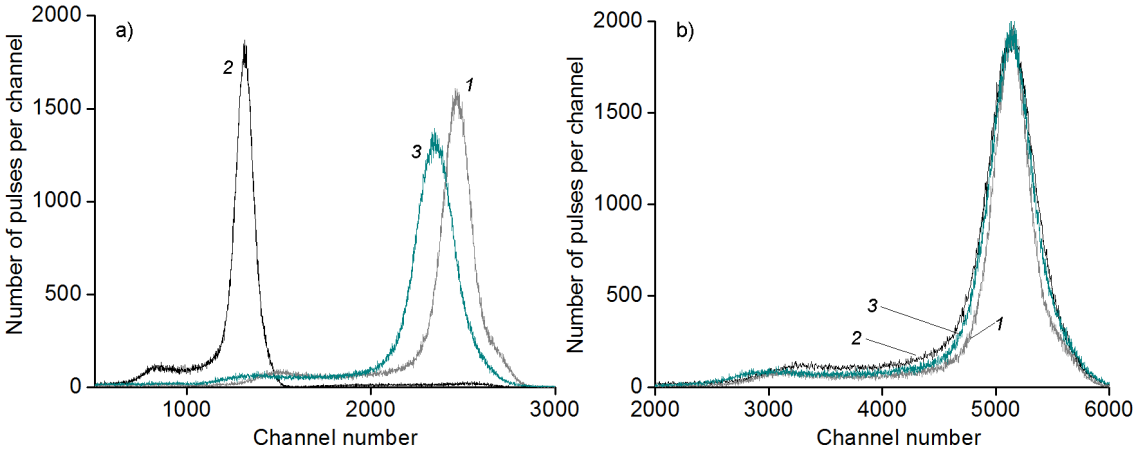

Fig. 7. Amplitude (a) and energy (b) spectra of $ZnS_{0.22}Se_{0.78}$ (*1*), ZnSe(Te) (*2*), and ZnSe(Al) (*3*) crystals obtained for α-particles from a ^{239}Pu source.

absorption edge to shorter wavelengths with increase of the sulfur content [31].

Light output is one of the main characteristics of scintillator, which determines its quality as a detector. The light output of ZnS_xSe_{1-x} plates was measured using X-ray excitation. The light output of ZnS_xSe_{1-x} bulk crystals excited by X-rays reached the level of ZnSe(Te) or even exceeded it. The light output of $ZnS_{0.22}Se_{0.78}$ (C3) plate was 1.6 times higher than the light output of ZnSe(Te) crystals (see Table 2).

Afterglow determines not only the inertia of the scintillator, but also the dynamic range of the recorded signals. The afterglow of ZnS_xSe_{1-x} plates was about 0.02 % after 15 ms except for $ZnS_{0.39}Se_{0.61}$ (C6) plate, for which it was equal to 0.07 % (see Table 2). This value is reasonably smaller as compared to afterglow of well-known scintillation materials such as ZnS, CsI(Tl), and Lu_2SiO_5:Ce [32–34].

3.5. Alpha radiation detection

In order to study the properties of ZnS_xSe_{1-x} crystals as alpha particle detectors a rectangular piece 10×10×2 mm^3 in dimensions was cut out from the $ZnS_{0.22}Se_{0.78}$ crystal, which was preliminary annealed in a Zn vapor (for the more details see [36]). For the sake of comparison, ZnSe(Al) and ZnSe(Te) crystals with the same dimensions and also annealed in a Zn vapour were used. The light output of ZnSe(Al), ZnSe(Te) and ZnS_xSe_{1-x} thin crystalline specimens was measured, by using the spectrometric methods and the ^{239}Pu alpha-particle source.

The energy position of registered peaks (Fig. 7a) testifies that the mixed $ZnS_{0.22}Se_{0.78}$ crystal has a higher light output in comparison with that of the ZnSe(Al) and ZnSe(Te) crystals. The $ZnS_{0.22}Se_{0.78}$ crystal also demonstrates a satisfactory separation (Fig. 7b) at energy of 5156 keV, which confirms the height efficiency of alpha-particle registration by the examined scintillator.

4. Conclusions

Among various A^2B^6 solid solutions, $ZnSe_{1-x}S_x$ crystals are of especial interest due to a wide possibility for tuning their properties, including scintillation ones. ZnS_xSe_{1-x} bulk crystals were grown by Bridgman-Stockbarger method in the range of $x = 0.07–0.39$. X-ray diffraction, optical absorption spectroscopy, scintillation emission spectroscopy were used for characterization of the plates. ZnS_xSe_{1-x} bulk crystals possess high optical quality. Concentration of sulfur was higher in fore of the crystal, segregation coefficients were in the range of 1.2–2.5. The scintillation properties of ZnS_xSe_{1-x} crystals depend on the sulfur content, best parameters were observed for $ZnS_{0.22}Se_{0.78}$ compound. Value of light output for $ZnS_{0.22}Se_{0.78}$ crystal measured in X-ray was by 1.6 times higher as compared to those of ZnSe(Al) crystal. Possibility of using ZnS_xSe_{1-x} bulk crystals as highly efficient X-ray detectors was revealed. Our researches also testify to the promising application of mixed ZnS_xSe_{1-x} crystals as alpha-particle detectors, with the $ZnS_{0.22}Se_{0.78}$ crystal having the best light yield and energy separation in the case where ^{239}Pu is applied as a source of alpha particles.

References

1. V.Ryzhikov, N.Starzhinskiy, L.Gal'chinetskii et al., *J. IEEE Nucl. Sci.*, **48**, 356 (2001).
2. A.I.Focsha, P.A.Gashin, V.D.Ryzhikov et al., *Inorg. Mater.*,, **3**, 1223 (2001).
3. M.Emam-Ismail, M.El-Hagary, E.Ramadan et al., *Radiat. Eff. Defect. S.*, **169**, 61 (2014).
4. N.Kolesnikov, E.B.Borisenko, D.N.Borisenko et al., *J. Cryst. Growth*, **401**, 849 (2014).
5. S.Cool, S.Miller, C.Brecher et al., *J. IEEE Nucl. Sci.*, **57**, 944 (2010).
6. N.G.Starzhinskiy, B.V.Grinyov, L.P.Galchinetskii et al., Institute for Single Crystals, Kharkov (2007).
7. A.Wagner, W.P.Tan, K.Chalut et al., *J. Cryst. Growth*, **456**, 290 (2001).
8. S.Usuda. *J. Nucl. Sci. Tech.*, **299**, 927 (1992).
9. K.Mochizuki, M.Takakusaki, *Phys. Status Solidi.A*, **94**, 243 (1986).
10. M.E.Ozsan, J.Woods, *Appl. Phys. Lett.*, **25**, 489 (1974).
11. Y.Shirakawa, H.Kukimoto, *Solid State Commun.*, **34**, 359 (1980).
12. N.B.Singh, C.H.Su, B.Arnold et al., *J. Opt. Mater.*, **60**, 474 (2016).
13. E.L.Trukhanova, V.I.Levchenko, L.I.Postnova, *Inorg. Mater.*, **50**, 10 (2014).
14. E.L.Barsukova, L.I.Postnova, V.I.Levchenko, *Crystallogr. Rep.*, **54**, 1245 (2009).
15. J.S.Prener, F.E.Williams, *J. Electrochem. Soc.*, **103**, 342 (1956).
16. J.S.McCloy, M.Bliss, B.Miller et al., *J. Luminescence*, **157**, 416 (2015).
17. V.B.Pham, T.T.Phan, *J. Sci.*, **24**, 181 (2008).
18. R.H.Hussein, O.Pages, F.Firszt et al., *J. Appl. Phys.*, **116**, 083511 (2014).
19. R.H.Hussein, O.Pages, S.Doyen-Schuler et al., *J. Alloy. Compd.*, **644**, 704 (2015).
20. R.H.Hussein, O.Pages, A.Polian et al., *J. Physics-Condens. Mat.*, **28**, 205401 (2016).
21. S.Fujita, H.Mimoto, H.Takebe et al., *J. Cryst. Growth*, **47**, 326 (1979).
22. GOST 17038.2-79 Scintillation Detectors of Ionizing Radiation. The Method of Measuring the Light Output of the Detector at the Peak of Total Absorption.
23. L.Vegard, *Z. Phys. A-Hadron. Nucl.*, **5**, 17 (1921).
24. T.Homann, U.Hotje, M.Binnewies et al., *Solid State Sci.*, **8**, 44 (2006).
25. S.Venkatachalam, D.Mangalaraj, S.K.Narayandass et al., *Semicond. Sci. Techn.*, **21**, 1661 (2006).
26. Y.Chen, J.Li, X.Yang et al., *J. Phys. Chem. C*, **115**, 23338 (2011).
27. K.B.Sundaram, G.K.Bhagavat, *J. Phys. D. Appl. Phys.*, **14**, 921 (1981).
28. O.G.Trubaieva, A.I.Lalayants, M.A.Chaika, UJP, **63**, 33 (2018).
29. A.B.Novoselova, V.B.Lazarev, Handbook, Moscow (1978) [in Russian].
30. P.Herve, L.K.J.Vandamme, *Infrared Phys. Techn.*, **35**, 609 (1994).
31. B.R.Pamplin, Crystal growth, Pergamon Press, New York (1975).
32. S.Larach, R.E.Shrader, C.F.Stocker, *Phys. Rev.*, **108**, 587 (1957).
33. V.D.Ryzhikov, N.G.Starzhinskiy, L.P.Gal'chinetskii et al., *Inorg. Mater.*, **3**, 1227 (2001).
34. N.N.Berchenko, V.E.Krevs, V.G.Sredni, Spreadsheets, Voenizdat, Moscow (1982) [in Russian].
35. A.M.Gurvich, Graduate School, Moscow (1971) [in Russian].
36. O.G.Trubaieva, M.A.Chaika, O.V.Zelenskaya, UJP, **63**, 546 (2018).